Optica Applicata, Vol. LIII, No. 4, 2023
DOI: 10.37190/oa230403

Practical Talbot wavemeter

NATTAWUT SUKSAWAT[1,2], SITTI BUATHONG[1,2], SARAYUT DEACHAPUNYA[1,2,3,*]

[1]Department of Physics, Faculty of Science, Burapha University,
ChonBuri Province, 20131, Thailand

[2]Quantum and Nano Optics Research Unit, Burapha University,
ChonBuri Province, 20131, Thailand

[3]Thailand Center of Excellence in Physics,
Ministry of Higher Education, Science, Research and Innovation,
328 Si Ayutthaya Road, Bangkok 10400, Thailand

[*]Corresponding author: sarayut@buu.ac.th

A wavemeter using the near-field Talbot diffraction is simplified. High accuracy wavelength measurement can be obtained from each spacing between two adjacent maximum intensities of the periodicity along multiples of the Talbot distance. Our experimental results are confirmed by our calculations. In contrast to the previous works, we use a diffraction grating with sufficiently large grating period. Therefore, the setup is practical and the pixel size of camera used to measure the interference pattern can be large. Moreover, the obtained Talbot patterns are sharp without using a post-image processing. According to our recent setup, we use the grating with a period of 12.5 μm. With visible light lasers, the Talbot distances are in the range of a few hundred of micrometers. These distances are much larger than a pixel size of normal camera. An external cavity diode laser with rubidium saturated absorption spectroscopy is used to calibrate our setup. High accuracy at 1 pm can be achieved.

Keywords: wavemeter, near-field effects, Talbot effect.

1. Introduction

Since first found by Henry Fox Talbot nearly two centuries ago [1], the Talbot effect, a self-imaging of periodic patterns in coherent optics, has been intensively studied. The effect involves a diffraction of monochromatic light via a periodic structure, such as a transmission grating, in a near-field regime where the wavefront curvature has to be taken into account and can be described by Fresnel diffraction. The self-image of a grating repeatedly appears at integer multiples of a distance so called the Talbot length L_T. Within the limit of the paraxial approximation, the Talbot length L_T can be expressed as $L_T = d^2/\lambda$ where d is the grating period and λ is the light wavelength. Moreover, rescaled Talbot self-images can be observed in fractions of the Talbot

length [2,3]. The Talbot phenomenon has been exploited in a wide range of applications from optical sensors [4-12] to matter-wave optics [13-16].

One of the promising applications of the Talbot effect is to utilize the Talbot effect for spectral measurement since coherent light sources with different wavelengths provide different Talbot periodicity of the self-images. Fourier-transform Talbot spectrometer was first experimentally demonstrated using a tilted grating [17]. The setup has no moving parts and can be compact in size. The spectral resolution is independent of the light wavelength, but limited by the grating period d. Another type of spectrometer with fixed optical elements was built using the Talbot effect in digital holography [18]. This spectrometer design is associated with the image amplitude reconstruction at different distances from a grating plane. The Talbot spectrometer based on a moving detector and slit was also proposed [19] and investigated for spectral responses to polychromatic white light [20]. Much improvement in wavelength resolution of tilted-grating Talbot spectrometers is recently obtained with the recent advances made in digital imaging sensors. A compact lens-free spectrometer using non-paraxial mid-field diffraction provides the spectral resolution less than 1 nm [21]. With the aid of tone parameter extraction algorithms, a compact Talbot wavemeter with below 10 pm precision was reported [22].

Here, a Talbot wavemeter based on measuring the Talbot length is proposed. An external-cavity diode laser (ECDL) locking to a rubidium saturated absorption spectrum of a rubidium vapor cell [23] is employed for calibration of the wavemeter. Thus, the spectral resolution of 1 pm is realized.

2. Methodology and experiment

Our Talbot wavemeter consists of a magnifying lens, grating and a camera (Fig. 1). The setup is similar to the previous work [22]. Nevertheless, the grating (d = 12.5 μm) with large grating period can be used in our scheme. Practically, a periodical grating with a larger period size provides advantages over the ones with smaller pitch since it

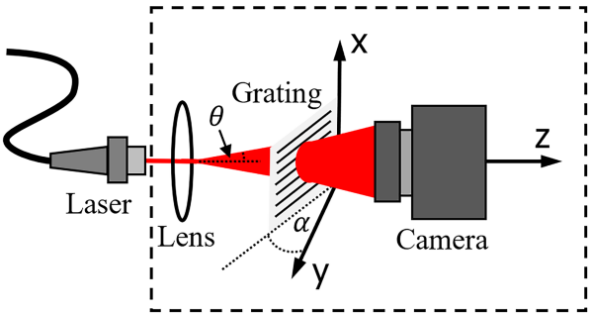

Fig. 1. Talbot wavemeter with an inclined grating configuration. The lens is used to expand the laser beam. A low-cost camera can be used to explore the Talbot interference patterns. The Talbot length, and therefore the laser wavelength, can be extracted from the interference patterns along the longitudinal direction (z) respected to the camera lines. The grating periodic structures are placed in the x-axis.

can bring about a larger detailed structure of an optical Talbot carpet. This makes an alignment process for the construction of a wavemeter and data analysis of the Talbot pattern much simpler. The lens (PAF2P-A10A, focal length = 10.0 mm, Thorlabs) is used to expand the laser beam to cover the entire area of the camera in order to achieve the highest possible number of Talbot carpet peaks. The distance between the lens and the grating is about 8 cm and between the grating and the camera is set to be a few mm in order to see sharp images. A low-cost camera (MT9J003 1/2.3-inch 10 Mp CMOS) with pixel size p of 1.67 μm can be used to explore the Talbot interference patterns. In order to obtain high accuracy to 1 pm, an external cavity diode laser (ECDL) [23] with rubidium saturated absorption spectroscopy is used to calibrate our setup. The calibration process is only required once during the installation of the wavemeter. The ECDL is a tunable laser and the wavelength of our laser used for calibration is λ_C = 780.241 nm because it can be locked to hyperfine spectra of Rb atoms with the D2 hyperfine transitions and the laser linewidth has been narrowed to below 100 kHz. The Talbot length obtained from two nearest peaks of the interference patterns along the longitudinal direction z respected to the camera lines (Figs. 2 and 3) is first calibrated with the ECDL. For divergent beam illumination ($\theta \approx 0.18°$), the Talbot distances will change with the number of Talbot plane or propagation distance [24,25]. However, this effect can be eliminated on our method as the laser calibration method can cancel out as shown in Eq. (1) as well as all uncertainties due to the parameters, such as grating period and tilt angle. The result of the wavelength measurement of an unknown laser λ can then be obtained,

$$\lambda = \frac{\lambda_C L_{\mathrm{T(C)}}}{L_{\mathrm{T}}} \tag{1}$$

where $L_{\mathrm{T(C)}}$ and L_{T} are the measured Talbot length of the calibrated laser (ECDL) and unknown laser, respectively.

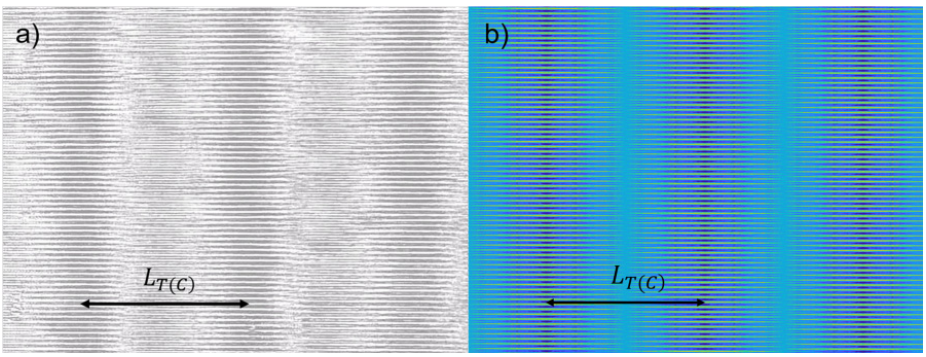

Fig. 2. An example of the experimental periodic pattern of the Talbot effect detected at a CMOS image sensor for a coherent light source of the ECDL (a). The Talbot length $L_{\mathrm{T(C)}}$ is also displayed along the z-axis due to the tilted grating. The simulation (b) done with $I(x, z) = \psi(x, z)\psi^*(x, z)$ from Eq. (2) with the grating tilted angle, α = 27.2°, divergent beam angle, $\theta \approx 0.18°$, and wavelength of 780.241 nm is used

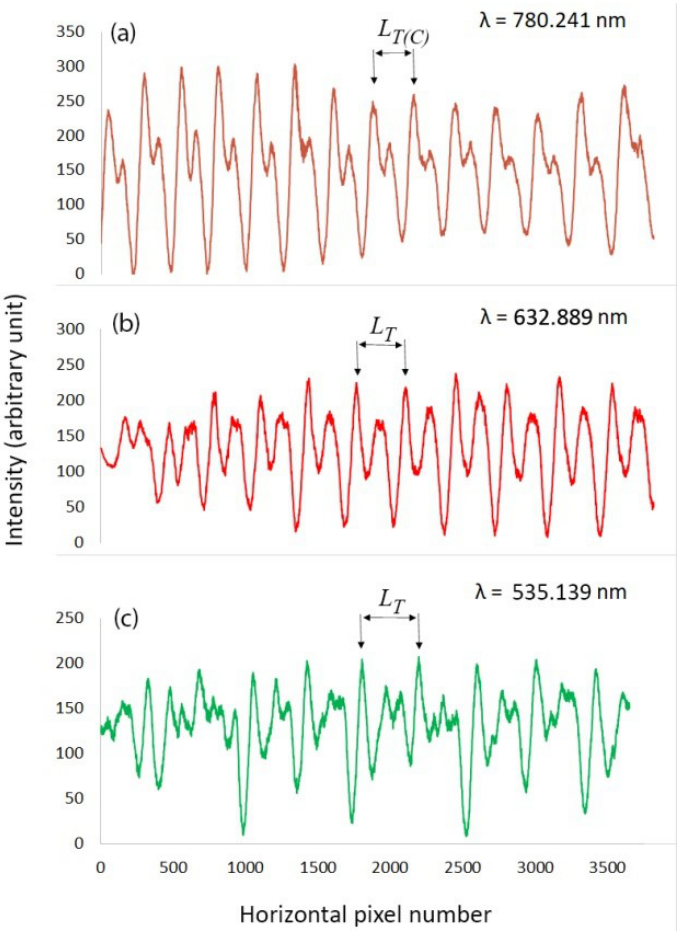

Fig. 3. Cross-section of the Talbot carpet (as shown in Fig. 2 for the laser wavelength of 780.241 nm) as a function of longitudinal (horizontal) pixels (z) for different laser wavelengths. (a), (b), and (c) are the cross-sections associated with the laser wavelength of 780.241, 633, and 532 nm (±10 nm), respectively. The arrows are shown for the examples of the peak positions used in measuring the Talbot length for each laser wavelength.

In order to check our experimental results, the wave on the detection screen, represented in the paraxial approximation with arbitrary angle of incidence θ is given by (for details see Ref. [3])

$$\psi(x, z) = \sum_n A_n \exp\left\{ i(k_\theta + nk_\mathrm{d})x + i\left[k - \frac{(k_\theta + nk_\mathrm{d})^2}{2k} \right] z \right\} \tag{2}$$

The Fourier components $A_n = \sin(n\pi f)/n\pi$ with f denoting the open fraction which is the ratio between the open window and period of the grating. The parameters $k_\theta = k\sin\theta$, $k_\mathrm{d} = 2\pi/d$, and $k = 2\pi/\lambda$ are the projection of the incident wave vector onto

the x-axis, wave number of the grating period, and wave number of the incident wave, respectively.

3. Methodology and experiment

The tilted transmission grating ($\alpha = 27.2°$) illuminated by coherent light leads to formation of the Talbot periodic structures, also called a Talbot carpet [3], at a detector. Figure 2 shows both an image of the Talbot carpet which was captured via an image sensor when the rubidium-stabilized ECDL with the wavelength of 780.241 nm was utilized as a light source and the simulation done with Eq. (2). The experimental result (Fig. 2(a)) fits well in great detail to our simulation (Fig. 2(b)). The grating period was located along the vertical pixels of the image and the horizontal pixels correspond to the longitudinal distance z from the transmission grating plane. Changes in intensity along the horizontal pixels are noticeably periodic. The Talbot length L_T can be measured from the regular intervals of these repeated patterns. This can be more evident via observing a cross-section over the horizontal pixels. The cross-sections for an ECDL at 780.241 nm, a He-Ne laser at 633 nm, and a green laser at 532 nm (±10 nm) were demonstrated and shown in Fig. 3. Each data point of the cross-section results from mean values of all rows of the Talbot carpet image. The distinctive peaks of the cross -section are indicated by the arrows shown in Fig. 3. The interference patterns shown in Figs. 2 and 3 were obtained directly and recorded from the camera without using a post-image processing. We use a programming for extracting the distance between the peaks of the Talbot distances. Our algorithm has a method of locking a threshold of selecting the spacing between the peaks. This can omit the peaks from fractional Talbot effect. The distances between these adjacent peaks in the unit of pixel size p were averaged to obtain the Talbot length L_T for a single Talbot carpet image. Thirty images of the Talbot carpet were analyzed for the measurement of each spectral wavelength of a laser to yield the final mean value of the Talbot length L_T. The ECDL was used as the reference laser since its output wavelength $\lambda_C = 780.241$ nm was frequency-locked to rubidium transition D2 line. The Talbot length $L_{T(C)}$ for the ECDL was detected to be $262p$ (p is the pixel size of the camera). The Talbot length L_T for the He-Ne laser and the green laser were measured to be $323p$ and $382p$. By using Eq. (1), the measured wavelengths of the He-Ne and green laser were 632.889 and 535.139 nm, respectively. These numbers can be obtained due to the accuracy of our calibration laser ($\lambda_C = 780.241$ nm). This is related to the systematic error of our setup [26]. These experimental results are in the typical range of both types of the lasers as specified in their datasheets. Nevertheless, we checked the He-Ne laser with the wavelength meter (WS7-60 Series, HighFinesse). The measured value was 632.992 nm, which corresponds to the value obtained by our wavemeter and can be varied with the laser temperature. The wavelength distribution was also measured at approximately 0.8 nm with a commercially available spectrometer (CCS175/M, Thorlabs). The statistical error of our measurements was about 0.9 nm due to the number of pixels. This can be improved by reducing the pixel size of the camera or increasing the Talbot pattern by a lens lo-

cating behind the grating. For example, if the pixel size is reduced by one order of magnitude, the statistical error can be 0.09 nm. Note that our experiment took place in an uncontrolled environment where there was no vibration reduction and temperature stabilization.

4. Conclusions

A simple wavemeter based on the near-field Talbot effect with large grating period has been demonstrated. A diffraction grating with large grating period can be used with our method. Therefore, the alignment and image processing can be made much easier. However, this simple technique is able to achieve high accuracy at 1 pm using the high precision laser calibration. The experimental samples were conducted with a low-cost diode laser and He-Ne laser. The obtained results were 535.139 and 632.889 nm, respectively. Measurement accuracy can be improved by using a higher precision and accuracy laser in the calibration process. This robust scheme has the potential to be used in scientific research such as atom tracking, laser locking and even for industrial applications.

Acknowledgements
This work was supported by the Thailand Center of Excellence in Physics (ThEP-60-PET-BUU8), the research unit grant from Faculty of Science and Burapha University (RU01/2565), and by Burapha University and Thailand Science Research and Innovation (TSRI) (Grant no. 24.1/2565).

References

[1] TALBOT H.F., *Facts relating to optical science*, Philosophical Magazine **9**, 1836: 401-407.
[2] BERRY M.V., KLEIN I.S., *Fractional and fractal Talbot effects*, Journal of Modern Optics **43**, 1996: 2139-2164.
[3] CASE W.B., TOMAND M., DEACHAPUNYA S., ARNDT M., *Realization of optical carpets in the Talbot and Talbot-Lau configurations*, Optics Express **17**, 2009: 20966-20974.
[4] SALAMA N.H., PATRIGNANI D., DE PASQUALE L., SICRE E.E., *Wavefront sensor using the Talbot effect*, Optics & Laser Technology **31**, 1999: 269-272.
[5] PRAKASH S., UPADHYAY S., SHAKHER C., *Real time out-of-plane vibration measurement/monitoring using Talbot interferometry*, Optics and Lasers in Engineering **33**, 2000: 251-259.
[6] LIU G., YANG C., WU J., *Characterization of Talbot pattern illumination for scanning optical microscopy*, Optical Engineering **52**, 2013: 091714.
[7] DEACHAPUNYA S., SRISUPHAPHON S., PANTHONG P., PHOTIA T., BOONKHAM K., CHIANGGA S., *Realization of the single photon Talbot effect with a spatial light modulator*, Optics Express **24**, 2016: 20029 -20035.
[8] PANTHONG P., SRISUPHAPHON S., PATTANAPORKRATANA A., CHIANGGA S., DEACHAPUNYA S., *A study of optical vortices with the Talbot effect*, Journal of Optics **18**, 2016: 035602.
[9] PANTHONG P., SRISUPHAPHON S., CHIANGGA S., DEACHAPUNYA S., *High-contrast optical vortex detection using the Talbot effect*, Applied Optics **57**, 2018: 1657-1661.
[10] PHOTIA T., TEMNUCH W., SRISUPHAPHON S., TANASANCHAI N., ANUKOOL W., WONGRACH K., MANIT P., CHIANGGA S., DEACHAPUNYA S., *High-precision grating period measurement*, Applied Optics **58**, 2019: 270-273.

[11] Liu Y., Zhang X., Huang Y., Zhang J., Hofmann W., Ning Y., Wang L., *Polarization stabilized VCSELs by displacement Talbot lithography-defined surface gratings*, Optik **183**, 2019: 579-585.
[12] Srisuphaphon S., Buathong S., Deachapunya S., *Simple technique for producing a 1D periodic intensity profile with a desired open fraction for optical sensor applications*, Journal of the Optical Society of America B **37**, 2020: 2021-2025.
[13] Berninger M., Stefanov A., Deachapunya S., Arndt M., *Polarizability measurements of a molecule via a near-field matter-wave interferometer*, Physical Review A **76**, 2007: 013607.
[14] Deachapunya S., Stefanov A., Berninger M., Ulbricht H., Reiger E., Doltsinis N.L., Arndt M., *Thermal and electrical properties of porphyrin derivatives and their relevance for molecule interferometry*, Journal of Chemical Physics **126**, 2007: 164304.
[15] Juffmann T., Truppe S., Geyer P., Major A.G., Deachapunya S., Ulbricht H., Arndt M., *Wave and particle in molecular interference lithography*, Physical Review Letters **103**, 2009: 263601.
[16] Cronin A.D., Schmiedmayer J., Pritchard D.E., *Optics and interferometry with atoms and molecules*, Reviews of Modern Physics **81**, 2009: 1051-1129.
[17] Kung H.L., Bhatnagar A., Miller D.A.B., *Transform spectrometer based on measuring the periodicity of Talbot self-images*, Optics Letters **26**, 2001: 1645-1647.
[18] Nicola S.D., Ferraro P., Coppola G., Finizio A., Pierattini G., Grilli S., *Talbot self-image effect in digital holography and its application to spectrometry*, Optics Letters **29**, 2004: 104-106.
[19] Lokshin G.R., Uchenov A.V., Éntin M.A., Belonuchkin V.E., Eskin N.I., *On the spectra selectivity of Talbot and Lau effects*, Optics and Spectroscopy **89**, 2000: 312-317.
[20] Guérineau N., Mambro E.D., Primot J., Alves F., *Talbot experiment re-examined: study of the chromatic regime and application to spectrometry*, Optics Express **11**, 2003: 3310-3319.
[21] Ye E., Atabaki A.H., Han N., Ram R.J., *Miniature, sub-nanometer resolution Talbot spectrometer*, Optics Letters **41**, 2016: 2434-2437.
[22] Han N., West G.N., Atabaki A.H., Burghoff D., Ram R.J., *Compact and high-precision wavemeters using the Talbot effect and signal processing*, Optics Letters **44**, 2019: 4187-4190.
[23] Thompson D.J., Scholtena R.E., *Narrow linewidth tunable external cavity diode laser using wide bandwidth filter*, Review of Scientific Instruments **83**, 2012: 023107.
[24] Rasouli S., Tavassoly M.T., *Application of the moiré deflectometry on divergent laser beam to the measurement of the angle of arrival fluctuations and the refractive index structure constant in the turbulent atmosphere*, Optics Letters **33**, 2008: 980-982.
[25] Azaña J., de Chatellus H.G., *Angular Talbot effect*, Physical Review Letters **112**, 2014: 213902.
[26] *ISO, IEC, OIML, BIPM. Guide to the Expression of Uncertainty in Measurement*, ISO, Geneva, 1995.

Received December 16, 2022